Enhanced Power Sharing Transient With Droop Controllers for Multithree-Phase Synchronous Electrical Machines

Alessandro Galassini , *Member, IEEE*, Alessandro Costabeber , *Member, IEEE*,
Michele Degano , *Member, IEEE*, Chris Gerada , *Member, IEEE*,
Alberto Tessarolo , *Member, IEEE*, and Roberto Menis , *Member, IEEE*

Abstract—**This paper presents a droop-based distributed control strategy for multithree-phase machines that provides augmented controllability during power sharing transients. The proposed strategy is able to mitigate the mutual interactions among different sets of windings without controlling any subspace variable, also offering a modular and redundant design. On the contrary, in a centralized configuration, subspaces would be controlled using the vector space decomposition, but fault tolerance and reliability levels required by the stricter regulations and policies expected in future transportation systems would not be satisfied. The proposed method is analytically compared against the state-of-the-art power sharing technique and equivalent models and control design procedures have been derived and considered in the comparison. Uncontrolled power sharing transients and their effects on mutual couplings among isolated sets of windings have been compared against the proposed regulated ones. Experimental results on a 22-kW nine-phase multithree-phase synchronous machine rig validate the design procedures showing good agreement with the expected performances.**

Index Terms—**Distributed power generation, motor drives, rotating machines, variable speed drives.**

I. Introduction

THE electrification of transportation systems started at the end of the 19th century. At that time, engineers already studied how to electrify many different technologies for a wide range of applications, like for example locomotives [1] and tractor ploughs [2]. Nevertheless, fossil fuel technologies superseded the electrification process during the 20th century. Only recently, thanks to many technology advancements (i.e., power

A. Galassini and A. Costabeber are with PEMC Group, University of Nottingham, Nottingham NG7 2RD, U.K. (e-mail: alessandro.galassini@nottingham.ac.uk; alessandro.costabeber@nottingham.ac.uk).
M. Degano, and C. Gerada are with the PEMC Group, University of Nottingham, Nottingham NG7 2RD, U.K., and also with the University of Nottingham, Ningbo 315000, China (e-mail: michele.degano@nottingham.ac.uk; chris.gerada@nottingham.ac.uk).
A. Tessarolo and R. Menis are with the University of Trieste, 34127 Trieste, Italy (e-mail: atessarolo@units.it; menis@units.it).

electronics, renewable energy sources, storage devices, etc.), following the resolution adopted by the general assembly of the United Nations held in 1989 [3], a proper propulsion system revolution aiming at pollution reduction has been launched. Since then, multiple research projects for transportation systems, i.e., mining machines [4], [5], ships [6], [7], offshore wind turbines [8], ultrahigh-speed elevators [9], road vehicles [10], and aircraft [11]–[13], have been founded by governments, innovation centers, and companies around the world.

Thanks to the ongoing electrical propulsion revolution together with the increase of high-power generation demand [14]–[16], multiphase electrical machines are gaining popularity [17], [18]. They present improved power density [19], reducing the current per-phase [20] without reaching the power electronics voltage limit [21]. Multiphase machines can guarantee higher fault tolerance and reliability levels [22] required by power systems for future aerospace and safety critical applications [23], [24]. Having multiple terminals, they can be wired within future on-board microgrids for more electric aircraft [25] introducing new redundant subsystem and power path in case of fault [26], [27]. Among all the on-board systems, which will be electrified, due to the required overloading and postfault operation capabilities, two of the most challenging ones are the engine [28] and the starter/generator [29].

Among multiphase machines, multithree-phase machines (MTPM) are a particular subgroup. They are obtained by winding multiphase machine phases into three-phase subwindings sets with isolated neutral points [30], [31]. Power-train redesign by adopting MTPM leads to modularity by extending redundancy from the power electronics to the control unit level. The repetition of independent modules made by one three-phase set of windings, one dc–ac two-levels three-phase voltage source inverter (2L-3P-VSI) (see Fig. 1), and one micro controller unit (MCU) will enable compliance with the forthcoming regulations in aerospace applications. Furthermore, the aforementioned repetition will allow the know-how on three-phase vector-control theory and fault management [32] to be reused, and eventually combined for developing new control strategies and postfault counter-measures [33]–[35].

In this paper, a power sharing transient regulator [36], [37] suitable for MTPM controlled by multiple independent modules is proposed, designed, and validated experimentally. The

Fig. 1. Dc–ac 2L-3P-VSI and one three-phase set of windings (*a, b, c*). d_a, d_b, d_c are the duty cycles.

Fig. 2. Centralized control architecture.

Fig. 3. CSR. Fully modular and redundant.

Fig. 4. CSR simplified control schematic with power sharing capabilities.

distributed power sharing controller is based on the very well-known droop regulator used in power systems [38]. If compared to the state-of-the-art power sharing regulator [39], [40], by having one MCU per module, the sharing transient controllability presented in this work improves the total harmonic distortion (THD) decreasing mechanical stress, vibrations, and electro-magnetic interferences (EMI) during the power sharing operation, but without compromising the overall system reliability.

This paper is organized as follows. In Section II, the two typical control configurations for MTPM are introduced and discussed. The conventional power sharing regulator and the proposed one are introduced in Sections III and IV, respectively. While showing their simplified equivalent models, they are compared in Section V. Before deriving the current sharing dynamics and its time constant in Section VII, control design procedures are given and compared in Section VI. Following two case studies in Section VIII, both the regulator designs are validated by means of experimental results in Section IX. Conclusions are drawn in Section X.

II. MULTIDRIVE CONTROL STRATEGIES

Based on how current is controlled within every set of windings, better performances or increased redundancy can be achieved [41], [42]. In Figs. 2 and 3, two different control configurations for MTPMs are shown. Every dc–ac converter output ($v_{a,b,c}$) is connected to one three-phase set of windings, $d_{a,b,c}$ are the duty cycles, $i^{\wedge}_{a,b,c}$ are the measured phase currents, and θ is the rotor position fed back from the speed sensor to the MCUs.

Thanks to the vector space decomposition (VSD), better current dynamics controlling all the orthonormal sub-spaces can be

achieved by the configuration in Fig. 2, in which all the measured currents are fed back into a single MCU. On the other hand, full redundancy is sacrificed in the name of lower THD [41], [42], in-fact, in case of faulty MCU, the entire system is compromised. Referring to Fig. 3 showing the common speed reference (CSR) configuration, having one MCU per dc–ac converter, gives a redundant system. Its main downside is from the controllability point of view. In fact, subspaces cannot be controlled because only the three local measured currents are fed back into every single MCU.

Considering the higher reliability and fault tolerance levels required by future aerospace systems, the CSR configuration is deemed to be the most suitable one in this paper, since modularity and redundancy are inherently achieved.

III. POWER SHARING—STATE OF THE ART

Among the features enabled by multithree-phase systems, for example, augmented reliability and fault tolerance at system level, one of the most interesting is power sharing. In Fig. 4, the CSR simplified control schematic with power sharing capabilities relative to Fig. 3 is shown. Each branch represents the q-axis within the rotating reference frame, ω^* is the speed set-point, and $\omega^{\wedge}$ is the measured speed. The continuous transfer functions $\omega_c/(s + \omega_c)$ represent the closed q-current loops with cutoff frequency ω_c and phase margin φ_c, whilst $(sK_{pS} + K_{iS})/s$ blocks are the speed proportional-integral (PI) controller transfer functions. Defining the number of modules N, the torque produced by the jth module T_j (with $j = 1 \dots N$), the jth q-current i_{qj}, and the machine constant $K_t = T_j/i_{qj}$, the total amount of

2

Fig. 5. Example of currents on phase a during power sharing transients (droop versus step).
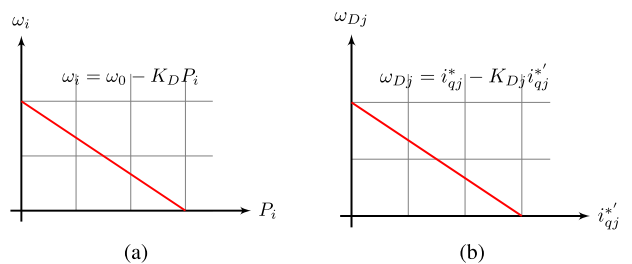

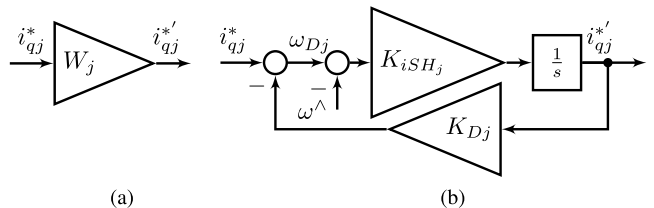Fig. 6. Droop planes comparison. (a) Droop plane in power systems. (b) Droop plane in motor control.

Fig. 7. Sharing regulator control diagrams comparison (a) Sharing coefficient. (b) Droop controller (G_{Dj}).

torque T_A produced by all the modules is set varying the q-current set-points i_{qj}^*. Introducing a sharing coefficient W_j, the jth q-current set-point, and therefore, T_j can be set. The sharing coefficients W_j define the new current set-points $i_{qj}^{*'}$ described by the following equation: $i_{qj}^{*'} = i_{qj}^* W_j$. In nominal conditions, power is equally split (ES) and loop gains are assumed to be equal to one, $W_{1,2,3}^{(ES)} = 1$. Depending on the particular application, unbalanced sharing (US) can be obtained varying the sharing coefficients.

In order to track the speed set-point ω^*, the total power P_{TOT} produced by all the modules must be kept constant. The total power is given by the sum of all the torques produced by each module multiplied by the shaft speed, $P_{TOT} = \sum_j^N T_j \omega$. Defining the *global sharing coefficient* $W_T = \sum_j^N W_j$, the power P_j in $p.u.$ produced by the jth module is described by the following equation:

$$P_j = \frac{I_{q,j}}{\sum_j^N I_{q,j}} = \frac{W_j}{W_T} \qquad (1)$$

where $I_{q,j}$ is the nominal current on the q-axis of the jth module. Thanks to (1), as long as W_T is kept constant, US can be achieved by just changing the sharing coefficients. Whenever US is needed, each W_j could be updated by a supervisory controller or programed offline *a priori* using the following formula:

$$W_j^{(US)} = P_j^{(US)} W_T \qquad (2)$$

and until the following equation is verified, constant speed loop dynamics is guaranteed

$$W_T = W_T^{(ES)} = W_T^{(US)} = \sum_j^N W_j = N. \qquad (3)$$

IV. ENHANCED POWER SHARING CONTROLLER

In this work, the droop controller is adopted for controlling the power sharing transient on an MTPM, and it is compared against the power sharing transient obtained by stepping the power sharing coefficients as previously discussed in Section III. As a qualitative example to anticipate the power sharing transients that will be shown later, Fig. 5 shows the same power sharing transient from 3 to 6 A processed by the power sharing coefficient and by the droop controller. It can be observed that the droop controller enables the power sharing transient

to be controlled by setting the time constant τ_{sh}, thus helping reducing vibrations and EMI.

Droop control is a very well-known technique adopted in power systems allowing the power demanded by the grid to be shared among different generators [38]. The droop characteristic is a linear function with negative coefficient K_D, called droop coefficient, on the *Frequency-Active Power* plane shown in Fig. 6(a) governed by [43]:

$$\omega_i = \omega_0 - K_D P_i \qquad (4)$$

where ω_i and ω_0 are the angular frequency of the output voltage and the nominal one, respectively, and P_i is the output active power [see Fig. 6(a)]. The greater the frequency, the less the power produced by the generation plant. Namely, when the frequency deviates from a certain value, the power produced varies according to the droop coefficient. Generated power can be therefore partitioned among different generation plants as a function of the droop gains [44].

In multithree-phase systems, the droop characteristic of the jth module [see Fig. 6(b)] is defined by the current reference i_{qj}^*, set by the speed regulator, and by the new current set-point $i_{qj}^{*'}$ according to

$$\omega_{Dj} = i_{qj}^* - K_{Dj} i_{qj}^{*'} \qquad (5)$$

where ω_{Dj} is an internal drooped set-point.

The control diagram relative to (5) is shown and compared against the sharing coefficient one in Fig. 7. Considering the control diagram in Fig. 7(b), the jth droop controller input–output relation is described by the following transfer function:

$$G_{Dj}(s) = \frac{K_{iSHj}}{s + K_{iSHj} K_{Dj}} = \frac{i_{qj}^{*'}}{i_{qj}^*} \qquad (6)$$

where K_{iSHj} is the integral droop coefficient. For simplicity, considering a system with only two modules, the *enhanced* CSR (*e*CSR) control diagram is shown in Fig. 8. The mechanical load
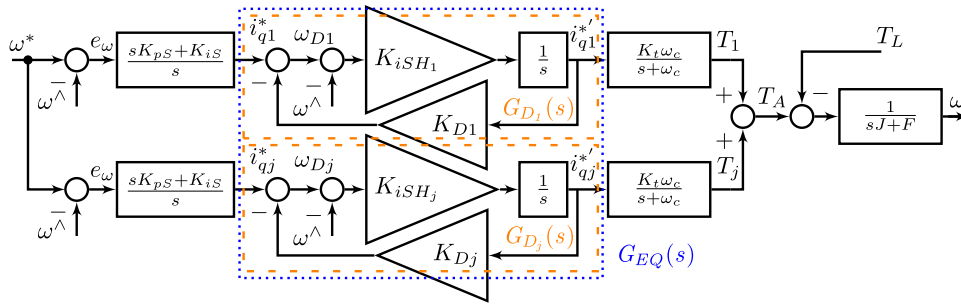
Fig. 8. CSR control diagram with *enhanced*, or droop, controllers (*e*CSR). For simplicity, only two modules are shown.

is common and it is represented by a linear model with inertia J and friction F. Like in Fig. 4, every q-current control loop is modeled as a low-pass filter with bandwidth ω_c and phase margin φ_c. In the *e*CSR configuration shown in Fig. 8, there are the following regulators.

1) PI q-current controllers

$$\mathrm{PI}_{Iq} = K_{pIq} + K_{iIq}/s \qquad (7)$$

within the q-current loops modeled by transfer functions $\omega_c/(s + \omega_c)$ as discussed in Section III;

2) Speed-drooped, or droop or sharing, controllers G_{Dj} shown in Fig. 7(b) characterized by bandwidth ω_{SH} and phase margin φ_{SH}, and described by (6);

3) PI speed controllers

$$\mathrm{PI}_S = (sK_{pS} + K_{iS})/s \qquad (8)$$

characterized by bandwidth ω_s and phase margin φ_s.

As it will be better explained in Section VI-B, the droop regulator should be designed considering the following constraint:

$$\omega_s < \omega_{SH} < \omega_c. \qquad (9)$$

A. Global Sharing Coefficient

In order to better understand Section VII, it is important to take into consideration the difference between steady-state gains of controllers from Fig. 7. For $s \to 0$, whilst the gain of the conventional controller is the sharing coefficient W_j itself, looking at (6) for $s \to 0$, the gain of the proposed droop controller G_{Dj} is $1/K_{Dj}$. The resulting global sharing coefficient for the droop controller is expressed by the following formula:

$$W_T' = \sum_j^N (1/K_{Dj}). \qquad (10)$$

B. Speed Drop

Considering the control diagram in Fig. 8, but without the outermost speed loops, the final speed of the shaft at steady state at no load ($T_L = 0$) can be calculated taking the limit for $s \to 0$, as shown in Fig. 9

$$\frac{\omega}{\omega^*} = \frac{\sum_j^N \frac{1}{K_{Dj}} K_t \frac{1}{F}}{1 + \sum_j^N \frac{1}{K_{Dj}} K_t \frac{1}{F}}. \qquad (11)$$
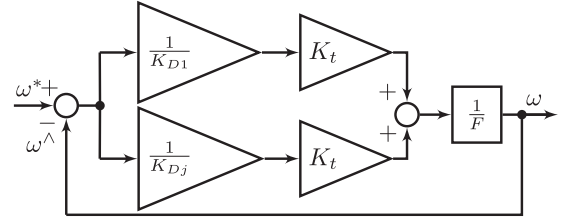
Fig. 9. *e*CSR without outermost speed loops at steady state while at no load for $s \to 0$.
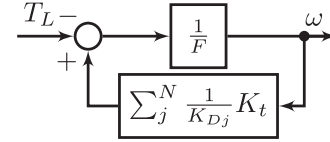
Fig. 10. *e*CSR without outermost speed loops at steady state with null speed reference for $s \to 0$.

Considering (10) and defining $\gamma = W_T' K_t / F$, (11) becomes:

$$\frac{\omega}{\omega^*} = \frac{\gamma}{\gamma + 1}. \qquad (12)$$

Similarly, according to the superposition principle, the torque contribution to the speed drop for a null speed reference can be calculated taking the limit for $s \to 0$, as shown in Fig. 10

$$-\frac{\omega}{T_L} = \frac{\frac{1}{F}}{1 + \frac{1}{F} \sum_j^N \frac{1}{K_{Dj}} K_t} = \frac{1}{F + W_T' K_t}. \qquad (13)$$

Combining (12) and (13), the final speed drop of the shaft at steady state is described by the following equation:

$$\omega = \omega^* \frac{\gamma}{\gamma + 1} - \frac{T_L}{F + W_T' K_t} \qquad (14)$$

Looking at Fig. 6, in power systems, the greater the power P_i produced by the ith generation plant, the less the angular frequency ω_i. In motor control, the greater the q-current set-point $i_{qj}^{*'}$, the less the internal drooped set-point ω_{Dj}. In other words, looking at Fig. 11, the greater the torque demand, the greater the speed drop defined as $\Delta\omega = \omega^* - \omega$. For a given maximum torque load T_{MAX}, the $\Delta\omega_{\mathrm{MAX}}$ would be the maximum speed drop if the outermost speed loops were not in place. When $T_L = 0\,\mathrm{N\cdot m}$, the second term in (14) is null, and only the friction F is contributing to the speed drop.
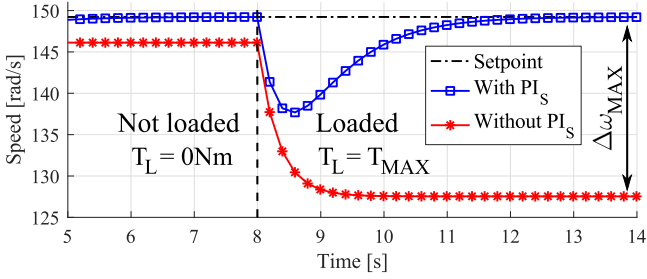
Fig. 11. Greater the torque demand, the greater the speed drop. At no load, only the friction is contributing to the speed drop.

V. SIMPLIFIED EQUIVALENT MODELS

In general, current regulators in MTPMs are designed on harmonic inductance and phase resistance values [45]. By definition, the first d and q harmonic inductances are mapped into the $\alpha - \beta$ plane and they are the inductances seen by the dc–ac converters under ideal and balanced voltage supply hypothesis [46]–[48]. The harmonic inductances can be obtained thanks to the VSD, and once they are computed, PI controllers along d- and q-axes can be designed taking into account actuation and filtering delays. The design of paralleled speed regulators shown in Figs. 4 and 8 is done assuming the power is ES among all the modules. Looking at Figs. 4 and 8, the jth speed controller output is the input reference i_{qj}^* for the jth sharing controller. In the following sections, reduced equivalent models for designing the speed controllers will be introduced.

A. Common Speed Reference

Looking at Fig. 4, and assuming the power is ES among the modules ($W_{1,2,3}^{(ES)} = 1$), the simplified equivalent model taking into account the N paralleled branches is shown and highlighted within dashed square in Fig. 13.

Design of the speed regulators PI_S can be done on the following plant:

$$G_S(s) = N \frac{\omega_c}{s + \omega_c} K_t \frac{1}{sJ + F}. \quad (15)$$

The same parameters $K_{pS}^{(CSR)}$ and $K_{iS}^{(CSR)}$ computed on plant in (15) can be used in the CSR simplified control schematic shown in Fig. 4.

B. Enhanced CSR

As shown in the previous section, speed and droop controller design has to be done on a plant considering the whole system and assuming equal power sharing ($K_{D_1}^{(ES)} = K_{Dj}^{(ES)}$ and $K_{iSH_1}^{(ES)} = K_{iSHj}^{(ES)}$). To this purpose, the control diagram in Fig. 8 can be simplified with the collective one shown in Fig. 12. The parallel of the N droop controllers $G_{Dj}^{(ES)}$ has been replaced by the equivalent collective droop controller

$$G_{EQ}(s) = NG_{Dj}^{(ES)}(s) \quad (16)$$

within the dotted blue square in Fig. 12. The constraint in (16) can be satisfied if and only if $K_{iSH} = K_{iSHj}^{(ES)}N$, and $K_D = $

$K_{Dj}^{(ES)}/N$, as highlighted by the following equation:

$$G_{EQ}(s) = \frac{NK_{iSHj}^{(ES)}}{s + K_{iSHj}^{(ES)}N\frac{K_{Dj}^{(ES)}}{N}} = NG_{Dj}^{(ES)}(s). \quad (17)$$

From (17), it can be verified that the whole system can be modeled as an equivalent single module with integral sharing gain K_{iSH} and droop gain K_D:

$$K_{iSH} = K_{iSH_j}^{(ES)}N \quad K_D = \frac{K_{Dj}^{(ES)}}{N}. \quad (18)$$

The K_D and the K_{iSH} gains in (18) can be defined as the collective droop and the collective integral gain coefficient, respectively. The equivalence in (16) can be further verified by plotting the Bode diagrams in Fig. 14.

Defining the following transfer function:

$$G_{SH_{OL}}(s) = G_{EQ}(s)\frac{\omega_c}{s + \omega_c} K_t \frac{1}{sJ + F} \quad (19)$$

therefore, speed regulator design can be done on the plant

$$G_{SH_{CL}}(s) = G_{SH_{OL}}(s)/(1 + G_{SH_{OL}}(s)). \quad (20)$$

Both transfer functions in (19) and (20) are highlighted in Fig. 12 by dashed red square and loosely dashed magenta square, respectively.

VI. CONTROL DESIGN PROCEDURES

Considering a system with N modules and with equal power sharing, design procedures for both control diagrams in Figs. 12 and 13 here are discussed and compared. It is important to notice that the dq-current loops denoted by low-pass filters $\omega_c/(s + \omega_c)$ and their design are the same for both control schemes. The plant used for designing the current PI regulators is expressed by (21). Measurement delay has been modeled by a second-order filter with cutoff frequency ω_{fc}, whilst actuation delay has been shaped as a pure delay $e^{-s1.5T_s}$, where T_s is the switching period. dq-current regulators are designed imposing bandwidth ω_c and phase margin φ_c on the following plant:

$$G_{I\Lambda}(s) = e^{-s1.5T_s} \frac{1}{s\Lambda_1 + r_s} \frac{\omega_{fc}^2}{s^2 + \sqrt{2}\omega_{fc}s + \omega_{fc}^2} \quad (21)$$

where r_s is the phase stator resistance, Λ stands for d or q, and Λ_1 is the first harmonic inductance along the d- or q-axis calculated using the VSD.

A. Common Speed Reference

Once the dq-current regulators are designed on plant $G_{I\Lambda}(s)$, speed regulators setting the sharing controller q-current references are designed on plant $G_S(s)$ in (15) considering the equivalent control scheme in Fig. 13. The same PI gains $K_{pS}^{(CSR)}$ and $K_{iS}^{(CSR)}$ can be used into control schematic in Fig. 4, where $W_{1,2,3}$ were assumed to be equal to one. While keeping constant the global sharing coefficient W_T in (3), power sharing can be then achieved by setting different sharing coefficient W_j thanks to (1) and (2).
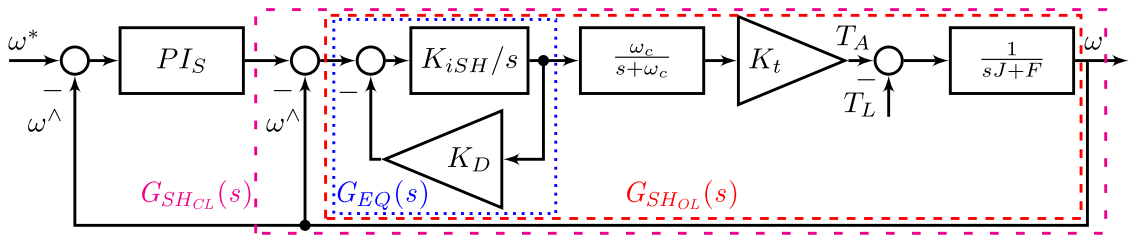
Fig. 12. Equivalent collective control scheme for the *e*CSR configuration assuming the power is ES among the N modules.
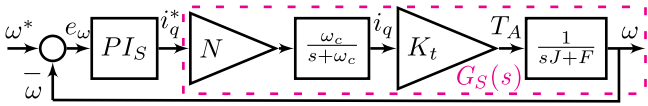

Fig. 13. Simplified equivalent model assuming sharing coefficients $W_{1,2,3}^{(\text{ES})} = 1$. For simplicity, the mechanical model is not shown in Fig. 4.
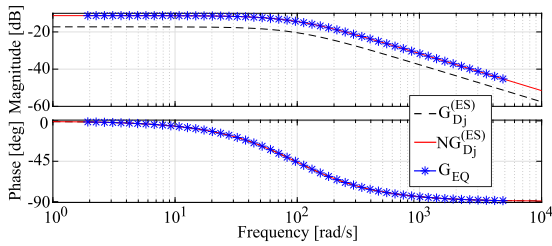

Fig. 14. Bode diagrams of transfer functions in (16).

B. Enhanced CSR

The introduction of droop controllers in between q-current and speed loops allows the power sharing transient to be regulated. The collective droop coefficient K_D must be chosen with the following equation:

$$K_D = \Delta\omega_{\text{MAX}}/I_{\text{TOT}} = \Delta\omega_{\text{MAX}}/\sum_j^N I_{q,j} \qquad (22)$$

where $\Delta\omega_{\text{MAX}}$ is the steady-state speed error without the outermost speed loops at full load, and $I_{q,j}$ is the nominal current on the q-axis of the jth module. Referring to Fig. 12, for a given sharing bandwidth ω_{SH} sufficiently slower than the current dynamics and faster than the outermost speed loop, in other words respecting (9), the collective integral gain K_{iSH} can be calculated imposing the phase margin φ_{SH} on (19), leading to the following analytical expression for the collective integral gain:

$$K_{iSH}$$
$$= \frac{\omega_{SH}}{\tan\left[-\varphi_{SH} + \pi - \text{atan}\left(\frac{\omega_{SH}}{\omega_c}\right) - \text{atan}\left(\frac{\omega_{SH} J}{F}\right)\right] K_D}. \qquad (23)$$

Under the previous hypothesis of balanced load and provided that $G_{EQ} = NG_{Dj}^{(\text{ES})}$, the same response of the designed equivalent collective system when using N modules can be achieved multiplying by N the collective droop gain and dividing by N the collective integral gain like in (18). Once the collective

sharing regulator is designed and its relative per-module coefficients $K_{D_j}^{(\text{ES})}$ and $K_{iSH_j}^{(\text{ES})}$ are computed, speed regulators design can be done considering the plant $G_{SH_{CL}}(s)$ in (20).

VII. DROOP SLOPES AND CURRENT SHARING DYNAMICS

Droop and speed loop regulators design is done under equal sharing hypothesis. If in the CSR configuration US is achieved changing $W_{1,2,3}^{(US)} \neq 1$ considering (3), in the *e*CSR configuration power sharing is achieved changing K_{D_j}. However, constant speed loop bandwidth and phase margins are guaranteed if and only if K_{iSH_j} are modified accordingly.

Defining $W_j' = 1/K_{Dj}$, the power in $p.u.$ produced by the jth module is described by the following equation:

$$P_j = \frac{I_{q,j}}{\sum_j^N I_{q,j}} = \frac{1/K_{Dj}}{\sum_j^N (1/K_{Dj})} = \frac{W_j'}{W_T'}. \qquad (24)$$

Comparing (24) against (1), in contrast to the CSR configuration, P_j is decreased by setting a bigger droop coefficient K_{Dj}. Viceversa, higher power is achieved with a smaller droop coefficient. Looking at (6), solely updating the droop coefficient would affect the droop controller transfer function frequency response, and therefore the collective one too. Equivalent droop controller constant frequency response is guaranteed if and only if the following condition is verified:

$$\sum_j^N G_{Dj}^{(\text{US})}(s) = NG_{Dj}^{(\text{ES})}(s) = G_{EQ}(s). \qquad (25)$$

On the assumption that $\sum_j^N P_j = 1$, (25) can be satisfied by dividing the individual equal power droop coefficients $K_{Dj}^{(\text{ES})}$ by a factor:

$$\xi_j = NP_j \qquad (26)$$

and multiplying the individual integral gain $K_{iSHj}^{(\text{ES})}$ by the same factor ξ_j. Combining (6) and (25):

$$\frac{NK_{iSHj}^{(\text{ES})}}{s + K_{iSHj}^{(\text{ES})}K_{Dj}^{(\text{ES})}} = \sum_j^N \frac{\overbrace{K_{iSHj}^{(\text{ES})}\xi_j}^{K_{iSHj}^{(\text{US})}}}{s + \underbrace{K_{iSHj}^{(\text{ES})}\xi_j}_{K_{iSHj}^{(\text{US})}}\underbrace{\frac{K_{Dj}^{(\text{ES})}}{\xi_j}}_{K_{Dj}^{(\text{US})}}}. \qquad (27)$$

TABLE I
SHARING CONTROLLER PARAMETERS

	CSR ($\tau_{sh,j}^{(CSR)} \to 0$)			Fast Sharing ($\tau_{sh,j}^{(f)} = 1[ms]$) $K_D^{(f)} = 0.5$ and $K_{iSH}^{(f)} = 2000$				Slow Sharing ($\tau_{sh,j}^{(s)} = 30[ms]$) $K_D^{(s)} = 0.5$ and $K_{iSH}^{(s)} = 66.\bar{6}$			
j	P_j	i_{qj}	W_j	P_j	i_{qj}	K_{Dj}	K_{iShj}	P_j	i_{qj}	K_{Dj}	K_{iShj}
Time: $0s \div 17.5s$ - **Equal Sharing (ES)** - ($K_{Dj}^{(ES)} = K_D N$ and $K_{iSHj}^{(ES)} = K_{iSH}/N$)											
$1,2,3$	$1/3$	2	1	$1/3$	2	1.5	$666.\bar{6}$	$1/3$	2	1.5	$22.\bar{2}$
$\sum$	1	6	$W_T = 3$	1	6	$W_T' = 2$	2000	1	6	$W_T' = 2$	$66.\bar{6}$
Time: $17.5s \div 20.5s$ - **Unbalanced Sharing (US)** - ($K_{Dj}^{(US)} = K_{Dj}^{(ES)}/\xi_j$ and $K_{iSHj}^{(US)} = K_{iSHj}^{(ES)}\xi_j$)											
1	$2/3$	4	2	$2/3$	4	0.75	$1333.\bar{3}$	$2/3$	4	0.75	$44.\bar{4}$
2	$1/12$	0.5	0.25	$1/12$	0.5	6	$166.\bar{6}$	$1/12$	0.5	6	$5.\bar{5}$
3	$1/4$	1.5	0.75	$1/4$	1.5	2	500	$1/4$	1.5	2	$16.\bar{6}$
$\sum$	1	6	$W_T = 3$	1	6	$W_T' = 2$	2000	1	6	$W_T' = 2$	$66.\bar{6}$
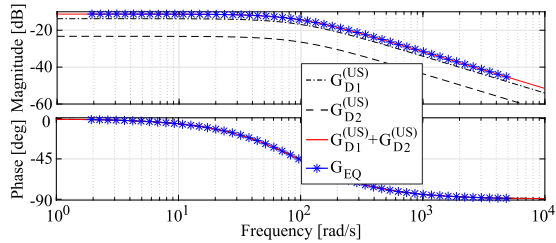
Fig. 15. Updating the integral gains K_{iSHj}, constant frequency response with different power ratios is guaranteed.

Equivalences in (25) and (27) are highlighted by their relative Blode plots in Fig. 15. The droop controller power sharing transient is ruled by the time constant $\tau_{sh,j}$ defined by the following equation:

$$\tau_{sh,j} = \frac{1}{K_{Dj}K_{iSHj}}. \qquad (28)$$

It is worth to notice that directly setting K_{Dj} and K_{iSHj} does not guarantee the overall system stability, therefore, it is recommended to design the droop controller with (22) and (23) by setting $\Delta\omega_{\text{MAX}}, \varphi_{SH}$, and ω_{SH}, while taking (9) into account.

Both the sharing controllers shown in Fig. 7 allow the power produced by every module to be set. However, whilst in the CSR control schematic shown in Fig. 4, the torque demand is set by the sharing coefficients W_j only, in the eCSR one shown in Fig. 8, the torque demand is set by the droop coefficients K_{Dj} and by the measured speed $\omega^\wedge$. The droop coefficient together with the integral gain sets the time constant $\tau_{sh,j}$ in (28). Power sharing with transient controllability could be obtained by simply adding a low-pass filter after the power sharing coefficients W_j shown in Fig. 4. In MTPM, the signal fed back to the MCUs is the speed of the only shaft within the system. However, if implemented on a multishaft application with elastic joint, the proposed sharing controller would self-adjust the torque demand of each module by taking into account the speed of every shaft. Furthermore, by feeding back another signal instead of the measured speed, the torque demand of each module could be set by an external factor.

VIII. CONTROL DESIGN—CASE STUDIES

In both CSR and eCSR configuration, current regulators have been designed considering the plant $G_{I\Lambda}(s)$ in (21). In the two following case studies, power sharing has been performed setting the following power ratios: $P_1 = 2/3$, $P_2 = 1/12$, and $P_3 = 1/4$.

A. Common Speed Reference

Assuming $W_{1,2,3} = 1$, speed controller for the CSR configuration has been designed on plant $G_S(s)$ in (15) leading to $K_{pS}^{(\text{CSR})}$ and $K_{iS}^{(\text{CSR})}$. Provided that $W_T = N = 3$, power sharing is achieved with (2) leading to the following sharing coefficients: $W_1 = 2$, $W_1 = 0.25$, and $W_3 = 0.75$, reported in Table I.

B. Enhanced CSR

Speed controller design has to be done after that the equivalent collective sharing controller $G_{EQ}(s)$ in (17) is arranged.

Thanks to (22) and (23), the resulting collective droop and integral coefficients can be computed. In order to highlight that the droop controller allows the power sharing time constant to be controlled, $G_{EQ}(s)$ will be designed two times with two different sets of design input parameters (ω_{SH} and φ_{SH}), labeled fast $^{(f)}$ and slow $^{(s)}$, respectively. Equations (22) and (23) are leading to the following collective coefficients: $K_D^{(f)} = K_D^{(s)} = 0.5$, $K_{iSH}^{(f)} = 2000$, and $K_{iSH}^{(s)} = 66.\bar{6}$. Once the equivalent sharing controller is obtained, the speed controller can be designed on the plant $G_{SH_{CL}}(s)$ in (20). Since the collective droop controller has been designed with two different sets of design input parameters [$G_{EQ}^{(f)}(s)$ and $G_{EQ}^{(s)}(s)$], two distinct sets of speed controller coefficients have been computed ($K_{pS}^{(f)}$, $K_{iS}^{(f)}$, $K_{pS}^{(s)}$, $K_{iS}^{(s)}$).

Per-module ES droop coefficients are then obtained by multiplying and dividing the collective gains by N like in (18), leading to the followings: $K_{Dj}^{(\text{ES},f)} = K_{Dj}^{(\text{ES},s)} = 1.5$, $K_{iSHj}^{(\text{ES},f)} = 666.\bar{6}$, and $K_{iSHj}^{(\text{ES},s)} = 22.\bar{2}$. The relative power sharing time constants can be obtained by (28) leading to $\tau_{sh,j}^{(f)} = 1$ ms and $\tau_{sh,j}^{(s)} = 30$ ms. Finally, per-module US sharing coefficients have
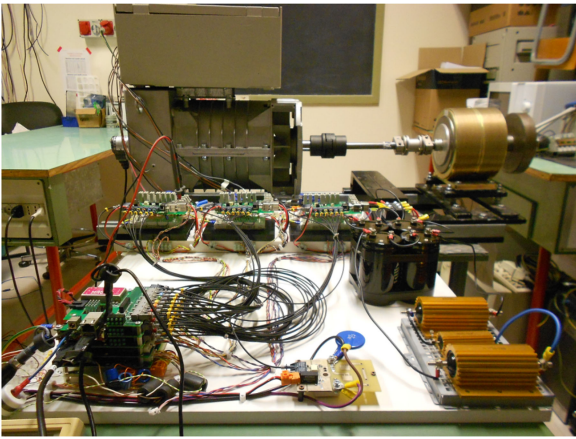
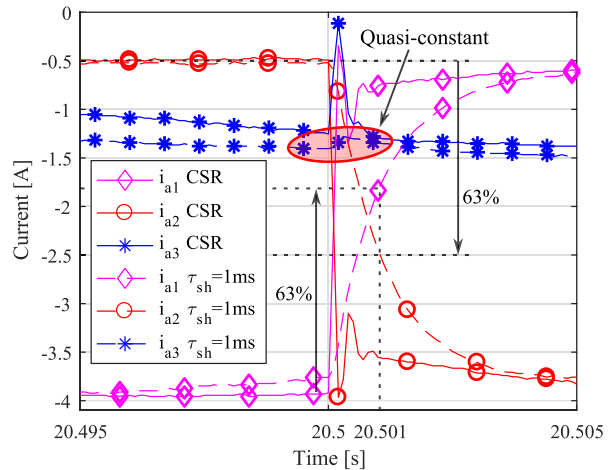Fig. 16.   Multithree-phase rig with nine phases.

Fig. 17.   CSR versus eCSR phase currents with $\tau = 1$ ms under swapping operation.

Fig. 18.   CSR versus eCSR phase currents with $\tau = 30$ ms under swapping operation.

been computed by putting the power ratios into (26), and then multiplying and dividing by ξ_j the integral and the droop coefficient, $K_{iSHj}^{(ES)}$ and $K_{Dj}^{(ES)}$, respectively, like in (27). All the sharing controller parameters are summarized in Table I.

IX. Experimental Validation

The droop controller has been validated on the experimental rig in Fig. 16. Every module was independently controlled by a custom control platform named μCube [49]. The MTPM with nine phases in Fig. 16 is a two poles synchronous generator derived by the SINCROGS14005001COD2FF514001 manufactured by Soga Energy Team. The brake coupled to the motor is a hysteresis brake from Magtrol. The converters have been built by combining the FP25R12KE3 power module from Infineon with the IRMD22381Q demo board for the relative IR22381Q gate drive, both from IOR. Switching and sampling frequency were both set to 10 kHz, braking torque generated by the hysteresis brake was 55.2 N·m, rotor field dc current was 1.58 A, and dc-link voltage was 350 V. On every module, the field oriented control has been implemented while controlling the d-current to zero like shown in Fig. 19, where saturation and speed filter blocks have been omitted for simplicity.

The measured output speed while performing power sharing with coefficients from Table I with modules in CSR mode is shown in Fig. 20(a). The q and their respective a phase currents from the three modules are plotted in Figs. 20(b) and (c), respectively. Until 17.5 s, having set $W_{1,2,3} = 1$, power was equally shared among the modules. From 17.5 and 20.5 s, sharing coefficients $W_{1,2,3}$ have been set equal to 2, 0.25, and 0.75, respectively. At instant 20.5 s sharing coefficients W_1 and W_2 have been swapped. Looking at Fig. 20(a), it is possible to verify that the speed is not affected by the power sharing and swapping operations.

In Fig. 21, measured speeds and q-currents from the modules configured in eCSR mode are shown. Looking at the measured output speeds during sharing and swapping operations for different time constants τ_{sh} shown in Fig. 21(a), it is possible to verify that the speed is not affected by the droop controllers. The q-currents under the same power sharing profile of Fig. 20(b) but with modules configured in eCSR mode with $\tau_{sh} = 1$ ms
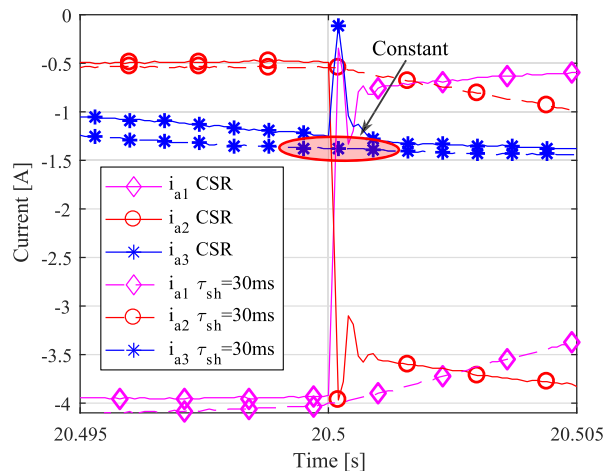
are shown in Fig. 21(b). In Fig. 21(c), the current transient in blue, labeled i_{q1}(CSR), and highlighted by the dashed oval in Fig. 20(b), is compared against the controlled current transients for different sharing time constants. The controlled transient plotted in red and labeled $i_{q1}\tau_{sh} = 1$ ms is highlighted by the dashed square in Fig. 21(b). The q-current steady-state values in Figs. 20(b) and 21(b), together with rise times in Fig. 21(c), are validating the control design procedures and the current sharing dynamics discussed in Sections VI and VII, respectively.

Phase a currents during swapping operations for $\tau_{sh} = 1$ ms and $\tau_{sh} = 30$ ms are zoomed in Figs. 17 and 18 . In both the plots, phase currents from the CSR (continuous lines) are compared against currents from the eCSR (dashed lines). Looking at both Figs. 17 and 18, the a current distortion from the third module, labeled i_{a3}(CSR), can be noticed. The distortion is caused by the mutual interactions among different sets of windings within the stator. In Fig. 17, the droop controller clearly mitigates the distortion caused by the electromagnetic coupling. By increasing the sharing time constant τ_{sh} to 30 ms, the third a current from quasi-constant it becomes constant, like highlighted by Fig. 18.
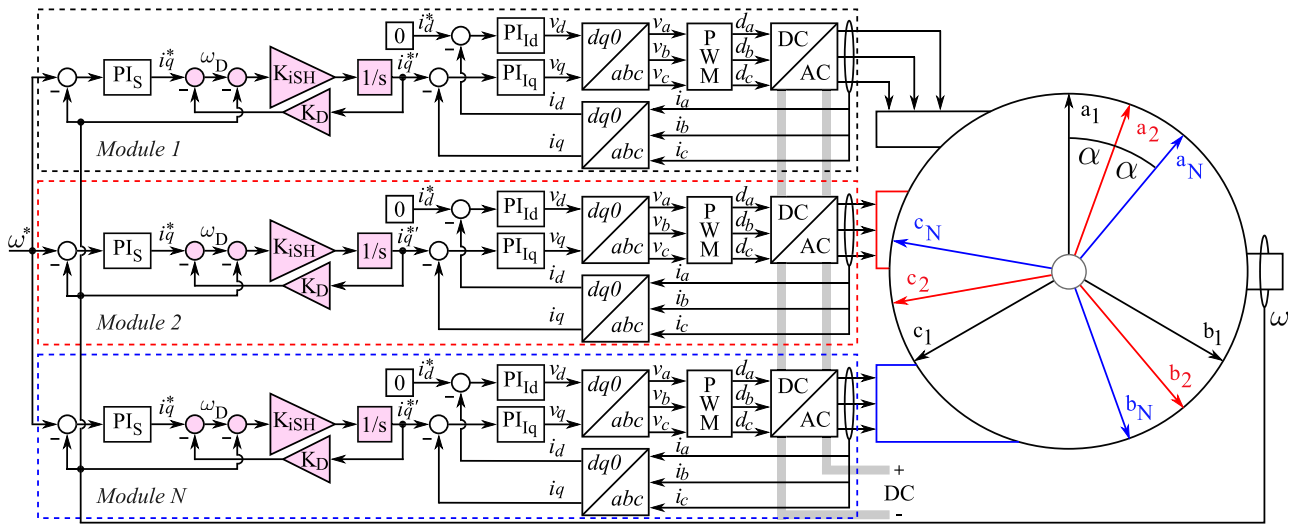
Fig. 19. Droop controller implementation. Speed filter and saturation blocks have been omitted for simplicity. Droop controllers are in magenta.
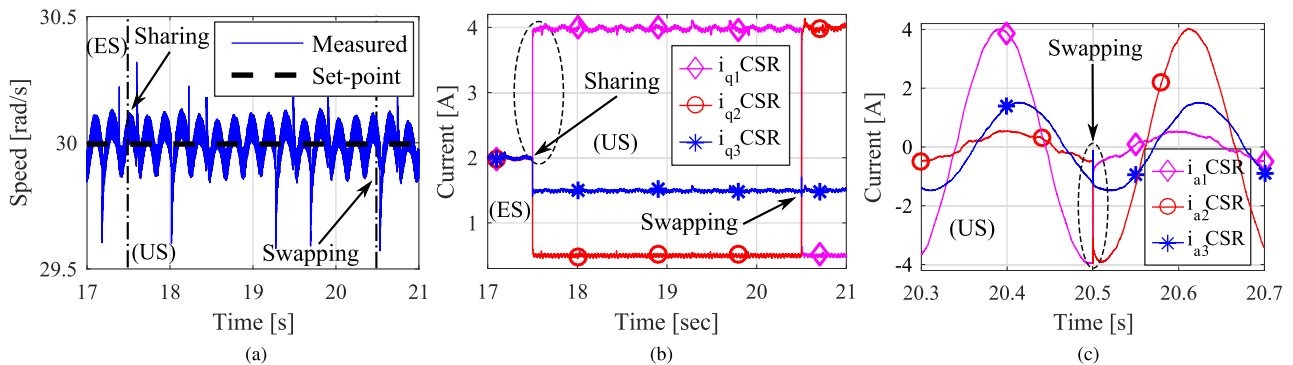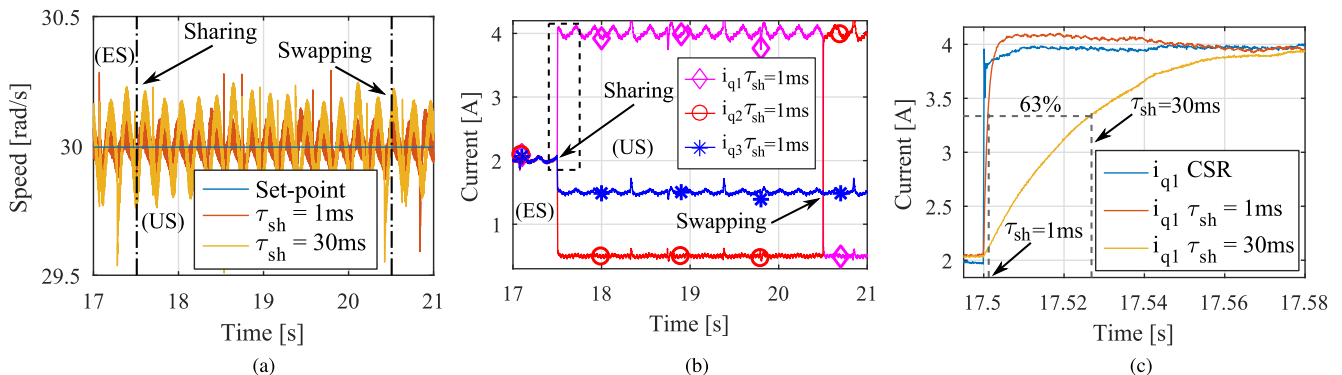

Fig. 20. CSR measurements. In Fig. 20(a), constant speed during sharing and swapping operation is highlighted. Uncontrolled q-current transients during sharing and swapping operations are shown in Fig. 20(b). In Fig. 20(c), respective a phase currents during swapping operation are shown. (a) Speed is not affected by load sharing. (b) q-currents under US conditions from CSR mode. (c) Phase a current transients while swapping $W_{1,2}$.

Fig. 21. eCSR measurements. In Fig. 21(a), constant speeds during sharing and swapping operation are highlighted. Respective controlled q-current transients with $\tau_{sh} = 1$ ms are shown in Fig. 20(b). Uncontrolled transient i_{q1} CSR is compared against the controlled ones in Fig. 21(c). (a) Measured speeds for different time constants, (b) iq currents from eCSR mode with $\tau_{sh} = 1$ ms, (c) CSR against eCSR for different time constants.

X. CONCLUSION

This paper was focused on the power sharing transient and its control design for multithree-phase electrical machines. The proposed enhanced distributed configuration allowed the power sharing time constant to be set, and during power sharing transients, current distortion due to the mutual interactions among different sets of windings was mitigated, thus reducing vibrations and EMI. Power sharing transient controllability was discussed and successfully verified after introducing the droop regulator for motor control applications. The droop controller and its characteristic were derived from the power system field

which is very well-known and widely adopted. Transfer functions, simplified equivalent models, Bode diagrams, and design procedures for both the CSR and the proposed eCSR configurations were provided and compared. The design procedures were validated and compared by means of analytical equations and experimental results on a 22-KW test rig showing good agreement with the expected dynamics. The proposed system appears to be a good subsystem for future power distribution system targeting at more reliable transportation systems and safety critical applications.

REFERENCES

[1] P. V. McMahon, "Electric locomotives in practice, and tractive resistance in tunnels, with notes on electric locomotive design," *J. Inst. Electr. Eng.*, vol. 28, no. 141, pp. 508–607, Aug. 1899, doi: 10.1049/jiee-1.1899.0027.

[2] R. B. Matthews, "Electric ploughing," *J. Inst. Electr. Eng.*, vol. 66, no. 383, pp. 1180–1190, Nov. 1928, doi: 10.1049/jiee-1.1928.0137.

[3] United Nations, "Protection of global climate for present and future generations of mankind," Jan. 1989. [Online]. Available: https://unfccc.int/sites/default/files/resource/docs/1989/un/eng/ares43 53.pdf?download

[4] M. G. Jahromi, G. Mirzaeva, S. D. Mitchell, and D. Gay, "Powering mobile mining machines: DC versus ac power," *IEEE Ind. Appl. Mag.*, vol. 22, no. 5, pp. 63–72, Sep. 2016, doi: 10.1109/MIAS.2015.2459082.

[5] G. Parise, L. Parise, A. Malerba, F. M. Pepe, A. Honorati, and P. B. Chavdarian, "Comprehensive peak-shaving solutions for port cranes," *IEEE Trans. Ind. Appl.*, vol. 53, no. 3, pp. 1799–1806, May/Jun. 2017, doi: 10.1109/TIA.2016.2645514.

[6] Z. Jin, G. Sulligoi, R. Cuzner, L. Meng, J. C. Vasquez, and J. M. Guerrero, "Next-generation shipboard dc power system: Introduction smart grid and dc microgrid technologies into maritime electrical networks," *IEEE Electrific. Mag.*, vol. 4, no. 2, pp. 45–57, Jun. 2016, doi: 10.1109/MELE.2016.2544203.

[7] G. Sulligoi, A. Vicenzutti, and R. Menis, "All-electric ship design: From electrical propulsion to integrated electrical and electronic power systems," *IEEE Trans. Transp. Electrific.*, vol. 2, no. 4, pp. 507–521, Dec. 2016, doi: 10.1109/TTE.2016.2598078.

[8] E. Prieto-Araujo, A. Junyent-Ferre, D. Lavernia-Ferrer, and O. Gomis-Bellmunt, "Decentralized control of a nine-phase permanent magnet generator for offshore wind turbines," *IEEE Trans. Energy Convers.*, vol. 30, no. 3, pp. 1103–1112, Sep. 2015, doi: 10.1109/TEC.2015.2412550.

[9] E. Jung, H. Yoo, S. K. Sul, H. S. Choi, and Y. Y. Choi, "A nine-phase permanent-magnet motor drive system for an ultrahigh-speed elevator," *IEEE Trans. Ind. Appl.*, vol. 48, no. 3, pp. 987–995, May 2012, doi: 10.1109/TIA.2012.2190472.

[10] G. Pistoia, *Electric and Hybrid Vehicles - Power Sources, Models, Sustainability, Infrastructure and the Market*. New York, NY, USA: Elsevier, 2010.

[11] B. Sarlioglu and C. T. Morris, "More electric aircraft: Review, challenges, and opportunities for commercial transport aircraft," *IEEE Trans. Transp. Electrific.*, vol. 1, no. 1, pp. 54–64, Jun. 2015, doi: 10.1109/TTE.2015.2426499.

[12] N. Nagel, "Actuation challenges in the more electric aircraft: Overcoming hurdles in the electrification of actuation systems," *IEEE Electrific. Mag.*, vol. 5, no. 4, pp. 38–45, Dec. 2017, doi: 10.1109/MELE.2017.2755266.

[13] J. Chen, C. Wang, and J. Chen, "Investigation on the selection of electric power system architecture for future more electric aircraft," *IEEE Trans. Transp. Electrific.*, vol. 4, no. 2, pp. 563–576, Jun. 2018, doi: 10.1109/TTE.2018.2792332.

[14] E. Levi, "Multiphase electric machines for variable-speed applications," *IEEE Trans. Ind. Electron.*, vol. 55, no. 5, pp. 1893–1909, May 2008, doi: 10.1109/TIE.2008.918488.

[15] M. J. Duran and F. Barrero, "Recent advances in the design, modeling, and control of multiphase machines - Part I," *IEEE Trans. Ind. Electron.*, vol. 63, no. 1, pp. 459–468, Jan. 2016, doi: 10.1109/TIE.2015.2448211.

[16] M. J. Duran and F. Barrero, "Recent advances in the design, modeling, and control of multiphase machines - Part II," *IEEE Trans. Ind. Electron.*, vol. 63, no. 1, pp. 459–468, Jan. 2016, doi: 10.1109/TIE.2015.2448211.

[17] E. Levi, "Multiphase ac machines," in *Power Electronics and Motor Drives* Electrical Engineering Handbook. Boca Raton, FL, USA: CRC Press, Feb. 2011, pp. 1–31. [Online]. Available: https://doi.org/10.1201/b10643-6

[18] R. Bojoi, S. Rubino, A. Tenconi, and S. Vaschetto, "Multiphase electrical machines and drives: A viable solution for energy generation and transportation electrification," in *Proc. Int. Conf. Expo. Electr. Power Eng.*, Oct. 2016, pp. 632–639, doi: 10.1109/ICEPE.2016.7781416.

[19] M. Farshadnia, M. A. M. Cheema, A. Pouramin, R. Dutta, and J. E. Fletcher, "Design of optimal winding configurations for symmetrical multiphase concentrated-wound surface-mount PMSMs to achieve maximum torque density under current harmonic injection," *IEEE Trans. Ind. Electron.*, vol. 65, no. 2, pp. 1751–1761, Feb. 2018, doi: 10.1109/TIE.2017.2745464.

[20] E. Levi, N. Bodo, O. Dordevic, and M. Jones, "Recent advances in power electronic converter control for multiphase drive systems," in *Proc. IEEE Workshop Electr. Mach. Design, Control Diagnosis*, Mar. 2013, pp. 158–167, doi: 10.1109/WEMDCD.2013.6525176.

[21] E. Levi, "Advances in converter control and innovative exploitation of additional degrees of freedom for multiphase machines," *IEEE Trans. Ind. Electron.*, vol. 63, no. 1, pp. 433–448, Jan. 2016, doi: 10.1109/TIE.2015.2434999.

[22] M. Barcaro, N. Bianchi, and F. Magnussen, "Faulty operations of a PM fractional-slot machine with a dual three-phase winding," *IEEE Trans. Ind. Electron.*, vol. 58, no. 9, pp. 3825–3832, Sep. 2011, doi: 10.1109/TIE.2010.2087300.

[23] W. Cao, B. C. Mecrow, G. J. Atkinson, J. W. Bennett, and D. J. Atkinson, "Overview of electric motor technologies used for more electric aircraft (MEA)," *IEEE Trans. Ind. Electron.*, vol. 59, no. 9, pp. 3523–3531, Sep. 2012, doi: 10.1109/TIE.2011.2165453.

[24] A. Pantea *et al.*, "Six-phase induction machine model for electrical fault simulation using the circuit-oriented method," *IEEE Trans. Ind. Electron.*, vol. 63, no. 1, pp. 494–503, Jan. 2016, doi: 10.1109/TIE.2015.2493727.

[25] A. Eid, H. El-Kishky, M. Abdel-Salam, and M. T. El-Mohandes, "On power quality of variable-speed constant-frequency aircraft electric power systems," *IEEE Trans. Power Del.*, vol. 25, no. 1, pp. 55–65, Jan. 2010, doi: 10.1109/TPWRD.2009.2031672.

[26] M. Pulvirenti, G. Scarcella, G. Scelba, M. Cacciato, and A. Testa, "Fault-tolerant ac multidrive system," *IEEE J. Emerg. Sel. Topics Power Electron.*, vol. 2, no. 2, pp. 224–235, Jun. 2014, doi: 10.1109/JESTPE.2013.2292861.

[27] B. Wang, J. Wang, A. Griffo, and B. Sen, "A general modeling technique for a triple redundant 3x3-phase PMA SynRM," *IEEE Trans. Ind. Electron.*, vol. 65, no. 11, pp. 9068–9078, Nov. 2018, doi: 10.1109/TIE.2018.2793229.

[28] M. Hirst, A. Mcloughlin, P. J. Norman, and S. J. Galloway, "Demonstrating the more electric engine: A step towards the power optimised aircraft," *IET Electr. Power Appl.*, vol. 5, no. 1, pp. 3–13, Jan. 2011, doi: 10.1049/iet-epa.2009.0285.

[29] S. Rubino, R. Bojoi, A. Cavagnino, and S. Vaschetto, "Asymmetrical twelve-phase induction starter/generator for more electric engine in aircraft," in *Proc. IEEE Energy Convers. Congr. Expo.*, Sep. 2016, pp. 1–8, doi: 10.1109/ECCE.2016.7854889.

[30] R. Dobler, T. Schuhmann, R. B. Inderka, and S. V. Malottki, "High performance drive for electric vehicles - system comparison between three and six phase permanent magnet synchronous machines," in *Proc. 18th Eur. Conf. Power Electron. Appl.*, Sep. 2016, pp. 1–10, doi: 10.1109/EPE.2016.7695475.

[31] M. Zabaleta, E. Levi, and M. Jones, "A novel synthetic loading method for multiple three-phase winding electric machines," *IEEE Trans. Energy Convers.*, to be published, doi: 10.1109/TEC.2018.2850976.

[32] B. Welchko, T. Lipo, T. Jahns, and S. Schulz, "Fault tolerant three-phase ac motor drive topologies: a comparison of features, cost, and limitations," *IEEE Trans. Power Electron.*, vol. 19, no. 4, pp. 1108–1116, Jul. 2004, doi: 10.1109/TPEL.2004.830074.

[33] M. Shamsi-Nejad, B. Nahid-Mobarakeh, S. Pierfederici, and F. Meibody-Tabar, "Fault tolerant and minimum loss control of double-star synchronous machines under open phase conditions," *IEEE Trans. Ind. Electron.*, vol. 55, no. 5, pp. 1956–1965, May 2008, doi: 10.1109/TIE.2008.918485.

[34] R. Bojoi, A. Cavagnino, A. Tenconi, and S. Vaschetto, "Control of shaft-line-embedded multiphase starter/generator for aero-engine," *IEEE Trans. Ind. Electron.*, vol. 63, no. 1, pp. 641–652, Jan. 2016, doi: 10.1109/TIE.2015.2472637.

[35] A. Galassini, A. Costabeber, and C. Gerada, "Speed control for multi-three phase synchronous electrical motors in fault condition," in *Proc. 17th Int. Conf. Smart Technol.*, Jul. 2017, pp. 698–703, doi: 10.1109/EUROCON.2017.8011200.

[36] A. Galassini, A. Costabeber, and C. Gerada, "Speed droop control of integrated modular motor drives," in *Proc. 41st Annu. Conf. IEEE Ind. Electron. Soc.*, Nov. 2015, pp. 003271–003276, doi: 10.1109/IECON.2015.7392604.

[37] A. Galassini, A. Costabeber, C. Gerada, G. Buticchi, and D. Barater, "A modular speed-drooped system for high reliability integrated modular motor drives," *IEEE Trans. Ind. Appl.*, vol. 52, no. 4, pp. 3124–3132, Jul. 2016, doi: 10.1109/TIA.2016.2540608.

[38] W. Allen J., W. Bruce F., and S. Gerald B., *Power Generation, Operation, and Control*. New York, NY, USA: Wiley, 1984.

[39] Allen-Bradley, "Load sharing applications for the 1336 impact ac drive," 1336E-WP001A-EN-P, Jun. 2000. [Online]. Available: http://literature.rockwellautomation.com/idc/groups/literature/documents/wp/drives-wp001_-en-p.pdf

[40] M. Mengoni *et al.*, "Control of a fault-tolerant quadruple three-phase induction machine for more electric aircrafts," in *Proc. 42nd Annu. Conf. IEEE Ind. Electron. Soc.*, Oct. 2016, pp. 5747–5753, doi: 10.1109/IECON.2016.7793968.

[41] Y. Hu, Z. Q. Zhu, and M. Odavic, "Comparison of two-individual current control and vector space decomposition control for dual three-phase PMSM," *IEEE Trans. Ind. Appl.*, vol. 53, no. 5, pp. 4483–4492, Sep. 2017, doi: 10.1109/TIA.2017.2703682.

[42] I. Zoric, M. Jones, and E. Levi, "Arbitrary power sharing among three-phase winding sets of multiphase machines," *IEEE Trans. Ind. Electron.*, vol. 65, no. 2, pp. 1128–1139, Feb. 2018, doi: 10.1109/TIE.2017.2733468.

[43] U. Borup, F. Blaabjerg, and P. Enjeti, "Sharing of nonlinear load in parallel-connected three-phase converters," *IEEE Trans. Ind. Appl.*, vol. 37, no. 6, pp. 1817–1823, Nov. 2001, doi: 10.1109/28.968196.

[44] J. M. Guerrero, J. C. Vasquez, J. Matas, L. G. de Vicuna, and M. Castilla, "Hierarchical control of droop-controlled ac and dc microgrids—A general approach toward standardization," *IEEE Trans. Ind. Electron.*, vol. 58, no. 1, pp. 158–172, Jan. 2011, doi: 10.1109/TIE.2010.2066534.

[45] J. Figueroa, J. Cros, and P. Viarouge, "Generalized transformations for polyphase phase-modulation motors," *IEEE Trans. Energy Convers.*, vol. 21, no. 2, pp. 332–341, Jun. 2006, doi: 10.1109/TEC.2005.859965.

[46] R. Bojoi, M. Lazzari, F. Profumo, and A. Tenconi, "Digital field-oriented control for dual three-phase induction motor drives," *IEEE Trans. Ind. Appl.*, vol. 39, no. 3, pp. 752–760, May 2003, doi: 10.1109/TIA.2003.811790.

[47] A. Tessarolo, L. Branz, and M. Bortolozzi, "Stator inductance matrix diagonalization algorithms for different multi-phase winding schemes of round-rotor electric machines part I. Theory," in *Proc. Int. Conf. Comput. Tool*, Sep. 2015, pp. 1–6, doi: 10.1109/EUROCON.2015.7313776.

[48] A. Tessarolo, L. Branz, and M. Bortolozzi, "Stator inductance matrix diagonalization algorithms for different multi-phase winding schemes of round-rotor electric machines part II. Examples and validations," in *Proc. Int. Conf. Comput. Tool*, Sep. 2015, pp. 1–6, doi: 10.1109/EUROCON.2015.7313777.

[49] A. Galassini, G. L. Calzo, A. Formentini, C. Gerada, P. Zanchetta, and A. Costabeber, "uCube: Control platform for power electronics," in *Proc. IEEE Workshop Electr. Mach. Design, Control Diagnosis*, Apr. 2017, pp. 216–221, doi: 10.1109/WEMDCD.2017.7947749.

Alessandro Costabeber (S'09–M'13) received the M.Sc. degree with honours in electronic engineering and the Ph.D. degree in information engineering with a focus on energy efficient architectures and control for future residential microgrids from the University of Padova, Padova, Italy, in 2008 and 2012, respectively.

In 2014 he joined the PEMC group at the University of Nottingham, U.K., as a Lecturer in Power Electronics. His current research interests include modular multilevel converters for HVdc, high power density converters, control and stability analysis of ac and dc microgrids.

Dr. Costabeber received the IEEE Joseph John Suozzi INTELEC Fellowship Award in Power Electronics in 2011.

Michele Degano (M'15) received the Laurea degree in electrical engineering from the University of Trieste, Trieste, Italy, in 2011, and the Ph.D. degree in industrial engineering from the University of Padova, Padova, Italy, in 2015.

In 2015, he joined the Power Electronics, Machines and Control Group, University of Nottingham, Nottingham, U.K., as a Research Fellow, where he is currently an Assistant Professor teaching advanced courses on electrical machines. His main research interests include design and optimization of permanent-magnet machines, reluctance and permanent-magnet-assisted synchronous reluctance motors through genetic optimization techniques, for automotive and aerospace applications.

Chris Gerada (M'05) received the Ph.D. degree in numerical modeling of electrical machines from the University of Nottingham, Nottingham, U.K., in 2005.

He subsequently worked as a Researcher with the University of Nottingham on high-performance electrical drives and on the design and modeling of electromagnetic actuators for aerospace applications. Since 2006, he has been the Project Manager of the GE Aviation Strategic Partnership. In 2008, he was appointed as a Lecturer in Electrical Machines; in 2011, as an Associate Professor; and in 2013, as a Professor with the University of Nottingham. His main research interests include the design and modeling of high-performance electric drives and machines.
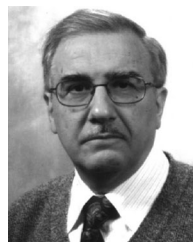
Prof. Gerada serves as an Associate Editor for the IEEE TRANSACTIONS ON INDUSTRY APPLICATIONS and is the past Chair of the IEEE IES Electrical Machines Committee.

Alberto Tessarolo (M'06) received the Laurea and Ph.D. degrees in electrical engineering from the University of Trieste, Trieste, Italy, in 2000 and 2011, respectively.

Before joining the university, he worked in the design and development of large innovative motors, generators, and drives with NIDEC-ASI (formerly Ansaldo Sistemi Industriali). Since 2006, he has been with the Department of Engineering and Architecture, University of Trieste, where he teaches the course of electric machine design.

Dr. Tessarolo serves as an Editor for the IEEE TRANSACTIONS ON ENERGY CONVERSION and Associate Editor for the IEEE TRANSACTIONS ON INDUSTRY APPLICATIONS and *IET Electric Power Applications*.

Alessandro Galassini (S'13–M'17) received the master's degree in mechatronic engineering from the University of Modena and Reggio Emilia, Reggio Emilia, Italy, in 2012, and the Ph.D. degree in power sharing for multithree-phase electrical machines from the University of Nottingham, Nottingham, U.K., in 2017.

He is currently a Researcher with the Power Electronics, Machines and Control Group, University of Nottingham. His research area is focused on control of electrical drives for future transportation systems.

Roberto Menis (S'79–M'92) received Single-Cycle Master's degree in electronic engineering, University of Trieste, Italy, 1982. He is with the Department of Engineering and Architecture, University of Trieste, Trieste, Italy, where he is currently an Associate Professor of Electric Drives. His research interests include the field of electric machines and drives: modeling, identification, and control of ac and dc machines, industry and transport applications of the drives, and dependability and functional safety for electrical systems.